Journal of Materials Chemistry A

PAPER

View Article Online
View Journal

Cite this: DOI: 10.1039/c9ta09088f

A novel flexible phase change composite with electro-driven shape memory, energy conversion/storage and motion sensing properties†

Malik Muhammad Umair,[a] Yuang Zhang,[a] Shufen Zhang,[a] Xin Jin[b] and Bingtao Tang *[ab]

In addition to their lower thermal conductivity, leakage during the melting phase and poor energy conversion ability, the fragility of phase change materials is an issue that is worth addressing to widen their application scope. Herein, we propose a low-cost and facile method to develop a flexible electro-driven phase change composite with unidirectional shape memory effects and motion detection properties. The phase change composite is composed of carbonized cotton cloth as a conductive supporting structure, paraffin wax as a latent heat storage material and thermoplastic polyurethane as a protective layer. The woven framework of carbonized cloth endowed the paraffin wax with the ability to generate Joule heating at a lower voltage due to its high electrical conductivity (374 S m^{-1}). The multifunctional layer of thermoplastic polyurethane wrapped the carbon cloth/paraffin and greatly improved the form-stability, flexibility and mechanical strength of the composite. Shape fixity and shape recovery properties of the composite were achieved by the synergic effect of the phase transition in paraffin and the elasticity of thermoplastic polyurethane. Moreover, the presence of conductive carbon cloth enabled the composite to achieve good electrothermal conversion efficiency and motion sensing properties. The fabricated flexible phase change composite may serve as a smart material for versatile thermal management applications.

Received 19th August 2019
Accepted 29th October 2019

DOI: 10.1039/c9ta09088f

rsc.li/materials-a

Introduction

Electro-thermal conversion materials are widely used for advanced thermal management applications.[1–4] The basic mechanism of electrothermal conversion is the generation of Joule heat by flowing electric current through a conductive material. As a suitable alternative to conventional metal-based electrothermal systems, carbon materials have gained considerable attention due to properties such as high conductivity and mechanical strength.[5,6] Carbon materials, such as carbon nanotubes (CNTs), graphene, and graphite, have been integrated with phase change materials (PCMs) to develop photothermal,[7,8] magnetothermal,[9,10] and electrothermal systems[11,12] for low-temperature applications. The use of PCMs in electrothermal systems is advantageous for the following reasons. (1) The isothermal phase changes of different PCMs can enable the adjustment of thermal regulation functions within the desired temperature range. (2) PCMs can absorb Joule heat while preventing convective heat dissipation and protecting the conductive structure from degradation. Several studies reported the synthesis and performance of electro-driven phase change composites supported by carbon supporting materials.[13–18] Porous carbon scaffolds are promising materials because they can encapsulate large amounts of PCMs and endow them with conductivity.[19–22] The high electrothermal conversion efficiency achieved by CNTs/eicosane,[23] graphene aerogel/paraffin,[24] and carbon foam/polyethylene glycol (PEG)[25] composites at low voltage demonstrates the impressive performance of porous carbon materials as Joule heaters. However, despite their form-stable and conductive properties, electro-driven phase change composites possess rigid structures. The lack of flexibility of phase change composites generally causes brittleness due to rigidity and may lead to poor installation due to the insufficient surface contact of the composite with the target application device. These issues hinder the use of phase change composites in developing flexible thermal management materials, such as thermal interface buffers, thermal blankets, wearable heaters, and thermal therapeutic devices.

The integration of PCMs in electrospun fibers and polymer matrices are feasible strategies to overcome its brittleness and achieve flexible composites. Electrospinning is the most widely used technique for generating flexible PCMs in the form of

[a]State Key Laboratory of Fine Chemicals, Dalian University of Technology, Dalian 116024, PR China

[b]Eco-chemical Engineering Cooperative Innovation Center of Shandong, Qingdao University of Science and Technology, Qingdao 266042, PR China. E-mail: tangbt@dlut.edu.cn

† Electronic supplementary information (ESI) available. See DOI: 10.1039/c9ta09088f

nanofibrous mats, coatings, and textiles.[26] However, this strategy presents two major deficiencies: (1) low encapsulation efficiency of PCMs, which leads to low latent heat storage, and (2) insufficient mechanical strength. In the second strategy, which uses a polymer matrix to induce flexibility, a literature survey indicates two significant approaches. In one approach, a commercially available polymer, that is, olefin *block*-copolymer, is used as a polymer matrix to encapsulate paraffin.[27,28] The resulting composites show thermally induced flexible behavior due to variations in the chain mobility of the polymer matrix triggered by the phase transition of paraffin. In another similar approach, a porous polymeric scaffold (melamine foam) is used to load paraffin.[29,30] The fabricated composites demonstrate shape memory functions because the phase change of paraffin enables the composite to regain its original position by restoring the elastic properties of the melamine foam. In these approaches, the fabricated composites exhibit thermal-activated flexibility, implying that they are solid composites below the melting point of paraffin. Therefore, attaining flexibility in both the solidified and melted states of PCM remains a focus of research because it can expand the scope of flexible PCM composites in versatile applications. However, achieving electrothermal conversion and flexible properties on a single platform in PCMs is still a challenge.

Given the above issues, a facile and low-cost strategy that intelligently combines the features of organic and inorganic materials with PCMs to design flexible composites was proposed. In the present study, a woven cotton cloth was carbonized at 900 °C, and the obtained carbon cloth (CC) containing hollow fibers served as a flexible supporting material.† The strong capillary forces of the interwoven carbon hollow fibers loaded the optimum amount of paraffin wax (PW) without showing leakage during phase changes. An efficient PCM-based Joule heating system was formed by the conductive pathways of well-aligned and highly graphitized CC. Furthermore, the interpenetrating layer of the thermoplastic polyurethane (TPU) coating successfully encapsulated the CC/PW, simultaneously enhancing the mechanical strength and flexibility of the composite. Moreover, the electro-driven CC/PW/TPU composite exhibited excellent shape fixity and recovery properties due to the combined effects of the phase transition of PW and the elasticity of TPU. The results of electrothermal energy conversion and strain-sensing performance of CC/PW/TPU provide insightful contributions to the development of smart thermoregulating devices.

Results and discussion

Fig. 1 illustrates the facile and low-cost fabrication strategy of the CC/PW/TPU composite. The cotton cloth was carbonized at 900 °C to obtain a porous network of interwoven carbon fibers (Fig. 2b and d). Due to the high surface area of CC, it is a suitable porous material to absorb small molecular PCMs, such as PW. Fig. 2b and e show the optimal amount of PW that completely diffused into the CC structure. Rapid diffusion occurred due to the strong capillarity of the highly aligned bundles of carbon fibers, which also restricted the PW seepage during phase changes. The use of the optimal amount of PW also left sufficient voids in the interwoven structure of CC for facile penetration and encapsulation by TPU (Fig. 2c and f). The morphological aspects of CC, CC/PW and CC/PW/TPU observed in the SEM analysis were reflected in the BET analysis of the respective samples (Fig. S1 and Table S1†). The BET results signified the high porosity of CC, whereas the optimal quantity of infiltrated PW in the porous CC left enough voids for the TPU coating to penetrate and encapsulate the woven network. The thickness of CC was 0.32 mm, and no layer was observed in CC/PW due to the complete diffusion of PW into the fibrous network of CC, as indicated by SEM and BET analysis. In CC/PW/TPU, the thickness of the composite reached 0.57 mm due to the TPU coating. The elemental carbon mapping of the samples indicated the graphitization of CC and the presence of PW in CC and the TPU coating on the composite (Fig. 2g–i). Thus, with a simple and scalable dip coating technique, the interpenetrating layer of TPU endowed CC/PW with flexibility and enabled the development of a novel flexible PCM composite.

After carbonization of cotton cloth, the obtained CC sample experienced surface area shrinkage of 49.12% and weight loss of 85.24% (Fig. 3a). To validate the carbonization of the cotton cloth, the degree of graphitization was assessed by X-ray photoelectron spectroscopy (XPS) survey spectra of pristine cotton and the carbonized cloth (Fig. 3b). The cotton cloth showed an elemental composition of 41.6% O and 58.4% C, which was supported by the energy-dispersive X-ray spectroscopy elemental mapping (Fig. S2†). In comparison, the XPS survey of CC showed high C content (93.82%) and low O content (6.24%). The degree of graphitization of the carbonized cloth was measured by Raman analysis. Fig. 3c shows two characteristic peaks at 1345 and 1598 cm^{-1}, which were ascribed to the D (disordered carbon structure) and G (graphitic carbon structure) bands, respectively. The high intensity of the G band compared with that of the D band signifies the presence of graphitic domains in the carbonized cloth.[31] The graphitic nature of CC was further confirmed by the X-ray diffraction (XRD) pattern of CC (Fig. 3d), which showed two broad and low-intensity peaks at 2θ positions of 21.9° and 44°; these can be indexed to the (002) and (100) spacings of the graphitized carbon structure, respectively. However, the present 2θ position

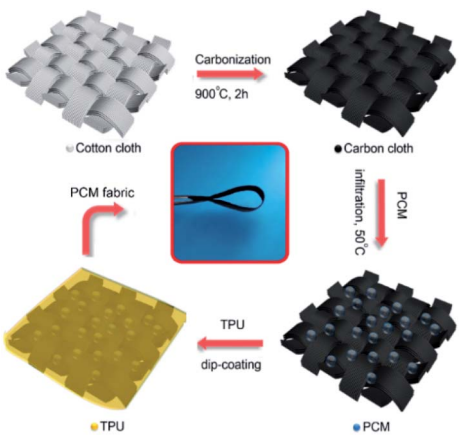

Fig. 1 Schematic of the fabrication of the CC/PW/TPU composite.

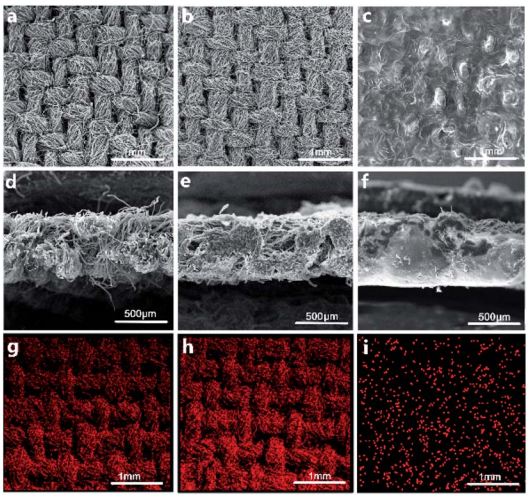

Fig. 2 SEM images of (a) CC, (b) CC/PW and (c) CC/PW/TPU with corresponding images of (d–f) a cross-section view and (g–i) elemental mapping showing the C content in CC, CC/PW and CC/PW/TPU.

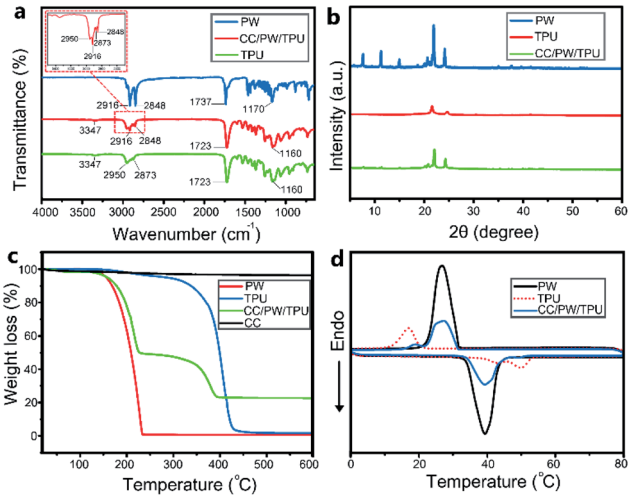

Fig. 4 (a) FTIR curves of PW, TPU and CC/PW/TPU. (b) XRD patterns of the PW, TPU, and CC/PW/TPU samples. (c) TG curves of PW, CC, TPU and the CC/PW/TPU composite. (d) DSC curves of PW, TPU and the CC/PW/TPU composite.

(21.9°) varied from the standard graphitic structure value (26.6°), indicating the broadening/expansion of interlayer spacing between the (002) planes. A similar phenomenon was previously reported for the synthesis of graphene-like carbon materials.[32] The above results signify the high degree of graphitization of CC and ascertain its conductive character.

Fourier-transform infrared (FTIR) spectroscopy was used to confirm the presence of TPU and PW in the composite. Fig. 4a shows the spectra of PW, TPU, and CC/PW/TPU. The PW spectrum contained characteristic peaks of hydrocarbon absorption bands at 2916 and 2848 cm^{-1}, whereas peaks at 1737 and 1170 cm^{-1} indicate the presence of free fatty acid vibrations. In the TPU spectrum, the typical peak at 3344 cm^{-1} denotes the stretching vibration of N–H bonds. The peaks at 2950 and 2873 cm^{-1} were assigned to symmetrical and asymmetrical stretching of –CH groups, respectively. The peaks at 1723 and 1160 cm^{-1} were attributed to the ester group (C=O) and carbonyl group (C–O) stretching vibrations, respectively, suggesting the polyester-based composition of TPU. The CC/PW/TPU composite exhibited not only the characteristic peaks of TPU but also the overlapping peaks of PW (2916 and 2848 cm^{-1}) without any shift, indicating the physical encapsulation of PW in the composite. This result was confirmed by the XRD analysis of the CC/PW/TPU composite (Fig. 4b). Sharp and intense diffraction peaks were observed at 7.3°, 11°, 14.7° 21.7°, and 24° in the XRD pattern of PW. The neat TPU exhibited characteristic peaks at 21.5° and 24.6°, whereas similar peaks of the constituents were recorded in the XRD pattern of the CC/PW/TPU composite. The low intensity of these peaks can be attributed to the low quantity of PW in the composite; also, they may be blocked by the pattern of amorphous CC.[33] The XRD analysis supports the FTIR results and indicates the physical interactions between the components of the composite.

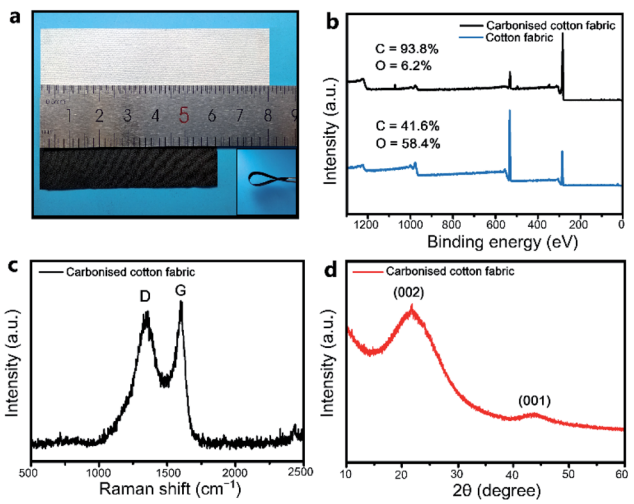

Fig. 3 (a) Photograph of pristine cotton cloth and CC showing the decrease in size after carbonization at 900 °C for 2 h. (b) XPS surveys of the pristine cotton cloth and CC showing the increase of the carbon content in the carbonized sample. (c) Raman spectrum and (d) XRD pattern of CC, indicating its graphitic character.

Thermogravimetric (TG) analysis was conducted to examine the practicality of the as-prepared CC/PW/TPU composite for thermal energy storage applications. Fig. 4c presents the TG curves of PW, CC, TPU, and the CC/PW/TPU composite. The TG analysis shows that CC exhibited almost no weight loss with increasing temperature, PW was thermally degraded between 150 °C to 225 °C, and thermal degradation of TPU occurred around 250 °C to 400 °C. The CC/PW/TPU composite exhibited two-stage thermal degradation behavior. The primary stage involved the degradation of PW in the temperature range of 200 °C to 250 °C. This increased thermal degradation temperature signifies the functionality of TPU as a protective barrier to decelerate the escape of vaporized PW. The secondary stage is attributed to the degradation of TPU, which is very similar to the

behavior of neat TPU. According to the TG data, the PW content in the composite reached 49.25%. These results show that the CC/PW/TPU composite satisfies the criterion of thermal stability required for practical applications. Moreover, the structure stability analyzed by form-stability tests further proved that CC/PW/TPU retained its solid state within the working temperature range without exhibiting any leakage or structural damage (Fig. S3†). The achieved form-stable properties can prevent damage caused by PCM leakage and can ensure the reliable performance of CC/PW/TPU for low-temperature applications (<50 °C)

The thermal energy storage and phase-transition performance of the CC/PW/TPU composite was determined by differential scanning calorimetry (DSC) data (Table S2†). The DSC curves in Fig. 4d show the onset melting temperature (T_m) of PW at 34.02 °C, with a melting enthalpy (ΔH_m) of approximately 196.30 J g^{-1}. Neat TPU exhibited two small endothermic peaks related to solid–solid phase changes at onset transition temperatures of 41.37 °C and 49.52 °C with negligible enthalpy values of 3.56 and 13.52 J g^{-1}, respectively. The DSC heating curve of CC/PW/TPU exhibited two transition peaks similar to those of pure PW and TPU, with onset transition temperatures of 34.13 °C and 48.99 °C, respectively. However, due to its low intensity, the endothermic peak of TPU at 48.99 °C was excluded from the calculations. The calculated melting enthalpy of the composite (93.56 J g^{-1}) was slightly lower than the theoretical melting enthalpy of 96.67 J g^{-1} (measured from 49.25% mass content of PW present in the composite through the TG data). The obtained thermal energy storage density of CC/PW/TPU (93.56 J g^{-1}) outperformed commercially available Outlast fabric (4 J g^{-1}) and PW@PU microcapsules embedded in Outlast/silk fabric (7.71 J g^{-1}).[34] Moreover, comparison with previously reported flexible PCM composites (Table 1) showed that the thermal storage properties of flexible CC/PW/TPU are reasonably good for practical applications.

Achieving desirable mechanical properties is crucial because pyrolysis of natural fibers causes substantial loss of tensile strength. The fragility of as-prepared CC can be subdued by encapsulation within a polymer matrix. Fig. 5a shows that the ultimate tensile strength of CC (0.16 MPa) was inferior to that of bare cotton cloth (1.09 MPa) (Fig. S4†). The ultimate tensile strength of CC was increased by the infiltration of PW (0.81 MPa) and later by the encapsulating layer of TPU (1.94 MPa). A slight decrease in the ultimate strength of CC/PW/TPU (1.41 MPa) was observed when it was heated above the melting temperature of PW. The tensile test results indicate that the polymer matrix of TPU had a positive effect on the tensile properties of the composite. Additionally, the interpenetrated TPU in the woven network of CC/PW provided satisfactory tensile strength below and above the phase change temperature of PW. As a result, the CC/PW/TPU composite showed exceptional bending and twisting deformation modes at room temperature (Fig. 5b). Moreover, the dynamic mechanical analysis (DMA) of CC/PW/TPU (Fig. S5†) recorded a loss of the storage modulus with increasing temperature. Also, around 50 °C, the solid–solid phase change of TPU occurred to a rubber-like elastic state. The demonstrated room temperature flexibility and mechanical robustness of CC/PW/TPU can offer ease of installation in confined spaces and on versatile shapes without a preheating step.

Table 1 Comparison of the thermal properties of previously reported flexible PCM composites and the CC/PW/TPU composite

Composite	PCM (wt%)	ΔH_m (J g^{-1})	Ref.
PAN/PW	54.3	60.31	35
PVA/PW	—	48.25	36
PVA/octadecane	15.0	4.3	37
PLA/dodecane	16.7	20.08	38
Silk/octadecane	14.2	37.58	39
PAN/isopropyl palmitate	28.0	27.2	40
PMMA/PW/CNT	40.0	58.25	41
CC/PW/TPU	49.25	93.56	This work

These results demonstrate the multifunctional role of TPU in enhancing the mechanical properties of the as-prepared PCM composites. Another important feature achieved by TPU encapsulation is the nonwetting surface of the composite. As shown in Fig. 5c and d, the temperature-dependent water contact angles of the composite recorded at room temperature and above the melting temperature range of PW demonstrated the influence of TPU on the surface hydrophobicity. The water droplets showed nonwetting behavior on the composite surface with a contact angle of around 126.5° at room temperature. Heating the CC/PW/TPU above the phase-change temperature range caused a slight decline in the contact angle (113 °C). The main contributing factor to this decline can be assigned to the continuous change in the TPU surface determined by the temperature-dependent contact angle measurement of CC/TPU (Fig. S6†). The nonwetting surface property of the composite during operating conditions can widen its application scope as a waterproof PCM fabric for thermal therapy or in e-textiles.

The electrical conductivity of any electro-driven system is dependent on the structure and conductance of the working

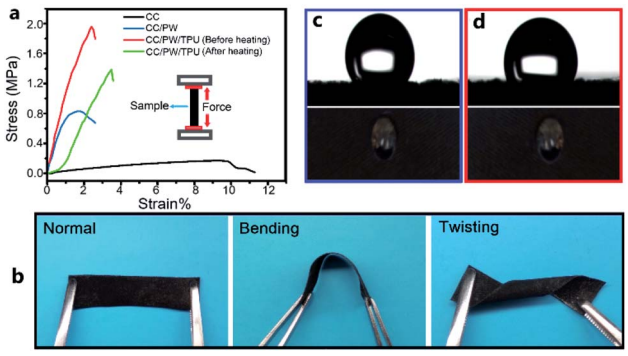

Fig. 5 (a) Stress–strain curves of CC, CC/PW, and the CC/PW/TPU composite before and after heating above the phase-change temperature (tests performed at a crosshead speed of 10 mm min^{-1}). (b) Digital images of normal, bending and twisting deformation modes of CC/PW/TPU at room temperature (solidified state). Contact angle measurements of CC/PW/TPU (c) at ambient temperature (20 °C) and (d) after heating above the phase-change temperature of PW with corresponding images of a 2 μL droplet on the composite surface.

components. A simple pyrolysis process transformed the cotton cloth into a well-aligned and flexible structure of interwoven conductive fibers for achieving high electrical conductivity, which is typically achieved by exclusively designing anisotropic carbon structures (*e.g.* graphene aerogel, 297 S m^{-1})[24] for preparing electro-driven PCMs. Fig. 6a shows a graphical display of the four-probe test measurements recorded at room temperature. The results show that the highly aligned and graphitic fibrous network of CC achieved excellent electrical conductivity (374.14 S m^{-1}), which consistently declined in the CC/PW (342.23 S m^{-1}) and CC/PW/TPU (296.68 S m^{-1}) composites due to the generated structural changes. In addition to the conductivity measurements, the *I–V* curves of CC (Fig. S7†) and CC/PW/TPU (Fig. 6b) passed through the origin of the coordinate system, indicating non-hysteretic ohmic behavior. The electrical conductance of CC/PW/TPU was also demonstrated by attaching a light-emitting diode (LED) to the composite. After the circuit was closed, the LED successfully lit up in normal and bent states, exhibiting the good structural stability of the flexible electro-conductive system (Fig. 6c and d). The Joule heating performance was demonstrated (Fig. 6e) by the application of stepwise voltage (2 to 3 V). The temperature of CC/PW/TPU increased at higher voltage as the CC generated a greater amount of resistive heat. At 2 and 2.5 V, temperature saturation was achieved, with a heating rate of around 0.13 °C s^{-1}. The temperature continuously increased at 3 V, and after the power was switched off, the temperature dropped at a rate of 0.75 °C s^{-1}. These excellent conductive properties manifest the potential of CC/PW/TPU for developing Joule heating devices and as a smart platform for designing flexible electronics.

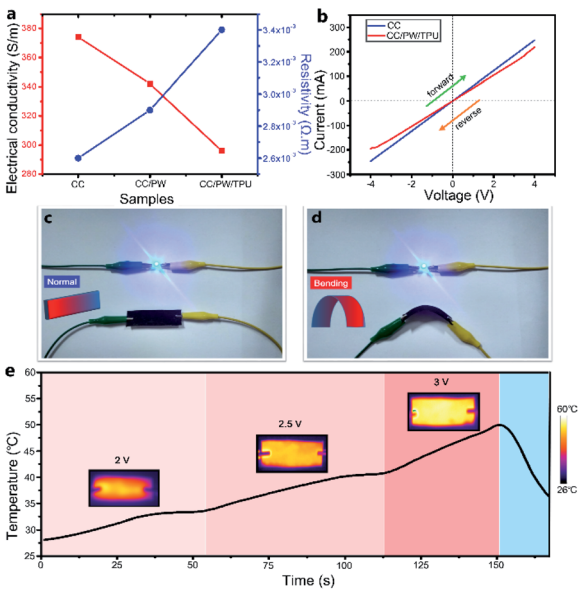

Fig. 6 (a) Graphical display of the electrical conductivity and resistivity values of CC, CC/PW and CC/PW/TPU. (b) *I–V* curves of CC/PW/TPU showing its ohmic character. LED lit by CC/PW/TPU patches in (c) normal and (d) deformed states under 3 V. (e) Temperature profile of the CC/PW/TPU patch under stepwise voltage (2 to 3 V).

The presence of conductive CC can be utilized to achieve electro-driven shape memory effects in as-prepared flexible composites. The introduction of the shape-memory effect is advantageous in PCM composites because it can overcome the difficulties of installation and minimum surface contact with the target material; these issues usually arise due to the rigidity of PCMs. The flexible CC/PW/TPU can effectively address these problems because it contains different components with distinctive physical and structural properties. The three main contributing features of CC/PW/TPU in establishing an effective electro-driven shape memory PCM composite were as follows: (1) the rigidity of PW enabled shape fixation, (2) the elasticity of TPU provided shape recovery, and (3) the conductive CC generated Joule heat under applied voltage to trigger shape recovery. Fig. 7a illustrates the basic shape memory mechanism of CC/PW/TPU. The composite was heated at 50 °C, manually deformed into a temporary shape, and cooled to ambient temperature (20 °C). Because the solidification temperature of PW was higher than the ambient temperature, PW solidification simultaneously overcame the resilience force of the coated TPU and maintained the sample in its temporary shape after the removal of the external force. To initiate the shape recovery process, the sample was connected to a DC power supply of 4 V. The Joule heat triggered the solid–liquid phase change in PW which softened the CC framework, while simultaneously the stored resilience force of TPU was released; this enabled the composite to regain its original shape, with a shape recovery ratio of almost 100%. Fig. 7b shows the rapid shape recovery in approximately the last 15 s, as demonstrated in Video S1.†

Based on the results of excellent electrical conductivity and good structural stability, the CC/PW/TPU composite can function as a flexible electrothermal conversion system. Well-aligned and interwoven conductive fibers of CC generated high Joule heating effects at 2, 3 and 4 V, which is evident from the rapid rise of the time–temperature curves (Fig. S8†). Moreover, upon removal of the electric voltage, the curves dropped quickly, indicating a high rate of heat discharge. Fig. 8a presents the electrothermal conversion performance of CC/PW/TPU evaluated at constant voltages of 2, 3, and 4 V. At an applied voltage of 2 V, temperature saturation was achieved, and phase-change platforms could not be observed within the given time. Evident and distinguishable phase-change platforms were observed at 3 and 4 V. The charging processes of CC/PW/TPU at 3 and 4 V lasted for 150 and 70 s, respectively, which spanned the range from room temperature to the end point of the

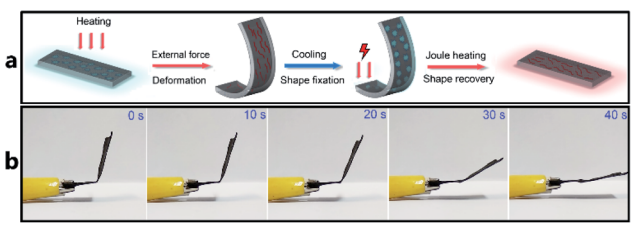

Fig. 7 (a) Illustration of the shape memory mechanism of CC/PW/TPU. (b) Photographs demonstrating the rapid electro-driven shape recovery of CC/PW/TPU to its original position.

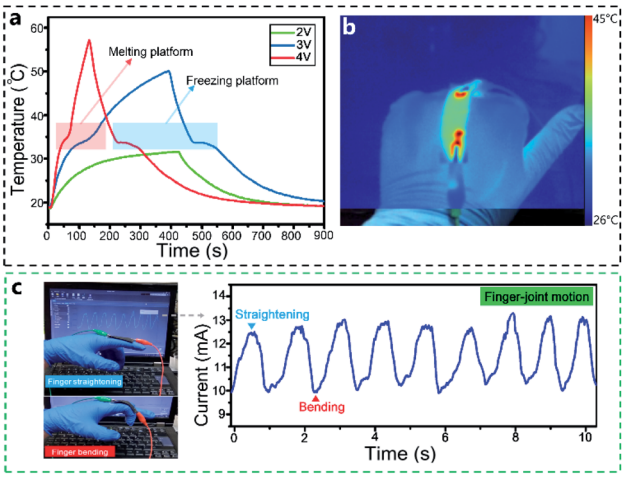

Fig. 8 (a) Electrothermal conversion curves of the CC/PW/TPU composite at constant voltage biases of 2 V, 3 V and 4 V. (b) CC/PW/TPU patch attached to a hand functioning as a flexible heater under 2.5 V. (c) Instantaneous electric signals in response to finger-joint straightening and bending, demonstrating the strain sensing activity of the flexible CC/PW/TPU patch.

melting platform. After completion of the melting platforms, the temperature increased continuously, and the composite absorbed the Joule heat as sensible heat. During the discharging process, the sensible heat quickly dissipated until a freezing platform was approached where the composite steadily released the latent heat energy. The discharging processes recorded from the freezing platform to room temperature lasted for 420 and 665 s under 3 and 4 V voltage bias, respectively. The locations of the phase-change platform in the electrothermal conversion curves were observed to be consistent with the results of the DSC analysis. Compared to CC, the prolonged heat discharging of CC/PW/TPU suggests that it more readily minimizes convective heat loss and should be preferably used as a thermal barrier layer for wearable thermal management (Fig. S9†). The electrothermal storage efficiencies of CC/PW/TPU at 3 and 4 V were measured as 34.88% and 67.39%, respectively. The increase in energy storage efficiency under a higher voltage is attributed to the shortening of the melting process, causing decreased heat loss from the heated composite (exposed to air) to the surroundings. The obtained storage efficiency of CC/PW/TPU is comparable with recently reported results for a graphene oxide/CNTs/PEG composite (66.3% under 7 V).[42] The electro-responsive CC/PW/TPU composite can function as a flexible Joule heater for low temperature (<50 °C) thermal management applications, as demonstrated in Fig. 8b.

Flexible strain sensors have gained enormous importance in motion detection for developing heat-monitoring, soft robotics, and smart electronics applications. The flexible conductive structure of CC/PW/TPU was utilized as a strain sensor by attaching the composite patch to a finger joint (Fig. 8c). The bending dynamic test simulated by finger-joint motion exhibited sharp electrical signals with good repeatability. The change in conductance upon finger motion was due to the stretching and relaxation of the fibrous network of CC, which caused a decrease and increase in the number of conductive contact points, respectively. These results highlight the potential use of the CC/PW/TPU composite as a flexible platform to integrate motion-sensing properties with electrothermal conversion for designing smart thermoregulating wearable systems.

Conclusions

In summary, we report a facile and rational strategy to prepare a flexible phase change composite containing cotton cloth-derived CC as a conductive supporting structure, PW as a latent heat storage material and TPU as a protective layer to encapsulate the PW/CC composite. The highly porous and well-aligned fibrous network of CC confined the PW through its strong capillarity. The phase change composites with PW loading as high as 49.25% exhibited good thermal stability and thermal energy storage density (93.5 J g^{-1}). The form-stable performance of CC/PW/TPU manifested the effectiveness of the leakage-proof flexible design. The bending and twisting deformation of CC/PW/TPU at room temperature demonstrated its flexible properties without the aid of thermal activation. Based on the test results, the mechanical and nonwetting surface properties of CC/PW/TPU in the working temperature range experienced an insignificant decline. The Joule heating of the CC structure executed an electro-driven shape-memory effect, with a shape recovery ratio of almost 100%. The distinctive ohmic characteristics of the electro-conductive CC were also evident in the fast charging speed of the phase change composite, with an electrothermal storage efficiency of 67.39% under a low voltage of 4 V. Moreover, the flexible conductive CC/PW/TPU also exhibited motion-detection properties through generating sharp electrical signals upon finger-joint movement. These promising results provide a future direction for designing new flexible PCM composites with thermal management and motion sensing functions.

Experimental

Materials

TPU in pellet form (polyester-based, MH-T80, density: 1.2 g cm^{-3}, MFI: 8–20) was purchased from the Shenzhen Fuxin Plastic Material Co., Ltd, China. Paraffin wax was procured from the Shanghai Joule Wax Industry Co., Ltd., China. Tetrahydrofuran (THF) and ethanol were supplied by Aladdin Chemicals, China. Cotton cloth was obtained from a local market.

Fabrication of the flexible phase change composite

Raw cotton fabric was washed with boiled water to remove any wax and impurities. A rectangular swatch of cotton cloth was cut in dimensions of 80 (l) × 30 (w) mm^2. The cotton swatch was placed in a ceramic crucible and transferred to a tubular furnace. The carbonization was carried out at a temperature rate of 5 °C min^{-1} and a stay time of 2 h at 900 °C. The obtained CC was washed with deionized water to remove ash and dried in a vacuum oven at 80 °C. The swatch of CC (72.5 mg) was placed in a Petri dish containing melted PW (72.5 mg), which quickly

diffused into the CC *via* strong capillary action. A solution of TPU was prepared in a beaker by dissolving 2 g TPU in 20 ml of THF solvent at room temperature. The TPU layer was coated on the obtained CC/PW composite by instantaneously immersing and removing it from the TPU solution. The obtained CC/PW/TPU (236.9 mg) composite was placed on a spiked platform and transferred to a vacuum oven to remove the solvent at 50 °C. After cooling the CC/PW/TPU composite to room temperature, a form-stable and flexible phase change material composite was obtained.

Electrothermal conversion setup

The rectangular sample was connected with two copper electrodes to obtain good electrical contact. Each electrode was connected through wires with a Keithley 2450 SourceMeter attached to the computer. The temperature measurements during the heating and cooling processes were recorded by attaching a temperature sensor (Pt100) to the data collection system. The same experimental setup was used for measuring the temperature-dependent tensile properties and contact angle by electro-heating. The electrothermal energy storage efficiency was measured as $\eta = m\Delta H/UI\Delta t$, where η is the ratio of stored heat [*i.e.*, the total mass of PW enclosed in the composite (m) times its enthalpy (ΔH)] to input the electrical energy during phase changes (*i.e.*, the product of the voltage (U), current (I), and time (Δt)]. The tangential method was used to determine the starting and terminating points of the phase changes located on the electrothermal conversion curves (Fig. S9†). The obtained time difference (Δt) was used in the energy storage efficiency equation.

Characterization

Scanning electron microscope (SEM) images of the surface morphologies and structures of the samples were obtained by an FEI Quanta 250 ESEM apparatus equipped with energy dispersive X-ray spectrometry (EDS). X-ray photoelectron spectra (XPS) were recorded on an ESCALAB250 multifunction surface analysis system with Al-Kα radiation. Raman spectra were obtained with a DXR microscope. FTIR analysis was carried out using a Nicolet 6700 FTIR spectrometer in ATR mode. The crystalline properties were analyzed using X-ray diffraction (XRD) patterns using a Rigaku D/Max 2400 (Japan) over a 2θ range of 5 to 60° at room temperature. Differential scanning calorimetry (DSC) was used to measure the thermal properties of the PCM composites using a DSC204 NETZSCH instrument (Germany) at a 5 °C min^{-1} heating rate under N_2 atmosphere. Thermogravimetric analysis (TGA) was carried out with a Universal Analysis TA2000 system at a heating rate of 10 °C min^{-1} under N_2 atmosphere from room temperature to 600 °C. Contact angle measurements were taken using a Powereach (JC2000D) instrument. A Fluke TiS75 Thermal Imager was used to record the heat distributions in the samples during the temperature-dependent tensile strength and contact angle measurements. The electrical conductivity and resistivity were measured by a 4-Probe Tech (RTS-9) meter. The dynamic mechanical properties were measured on a DMA 1 (METTLER TOLEDO) dynamic mechanical analyzer. Nitrogen adsorption and desorption analysis was conducted on a BeiShiDe 3H-2000PM specific surface and pore size analyzer at 77.3 K.

Conflicts of interest

There are no conflicts to declare.

Acknowledgements

This work was supported by the National Natural Science Foundation of China (21576039, 21878043, 21276042, 21421005 and U1608223), Program for Innovative Research Team in University (IRT_13R06), Fundamental Research Funds for the Central Universities (DUT18ZD218), Talent Fund of Shandong Collaborative Innovation Center of Eco Chemical Engineering (XTCXYX04), and Program for the Innovative Talents of Higher Learning Institutions of Liaoning (LCR2018066).

Notes and references

1 Y. Zhang, M. M. Umair, S. Zhang and B. Tang, *J. Mater. Chem. A*, 2019, **7**, 22218–22228.
2 R. Zhou, P. Li, Z. Fan, D. Du and J. Ouyang, *J. Mater. Chem. C*, 2017, **5**, 1544–1551.
3 Y. Yao, K. K. Fu, C. Yan, J. Dai, Y. Chen, Y. Wang, B. Zhang, E. Hitz and L. Hu, *ACS Nano*, 2016, **10**, 5272–5279.
4 S. Hong, H. Lee, J. Lee, J. Kwon, S. Han, Y. D. Suh, H. Cho, J. Shin, J. Yeo and S. H. Ko, *Adv. Mater.*, 2015, **27**, 4744–4751.
5 Y. Liu, Y. Yang and S. Li, *J. Mater. Chem. A*, 2016, **4**, 18134–18143.
6 H. Lei, C. Fu, Y. Zou, S. Guo and J. Huo, *J. Mater. Chem. A*, 2019, **7**, 6720–6729.
7 X. Fan, L. Liu, X. Jin, W. Wang, S. Zhang and B. Tang, *J. Mater. Chem. A*, 2019, **7**, 14319–14327.
8 Y. Zhang, M. M. Umair, X. Jin, R. Lu, S. Zhang and B. Tang, *J. Mater. Chem. A*, 2019, **7**, 8521–8526.
9 W. Wang, X. Fan, J. Qiu, M. M. Umair, B. Ju, S. Zhang and B. Tang, *Chem. Eng. J.*, 2019, **358**, 1279–1286.
10 W. Wang, M. M. Umair, J. Qiu, X. Fan, Z. Cui, Y. Yao and B. Tang, *Energy Convers. Manage.*, 2019, **196**, 1299–1305.
11 Z. Zheng, J. Jin, G.-K. Xu, J. Zou, U. Wais, A. Beckett, T. Heil, S. Higgins, L. Guan, Y. Wang and D. Shchukin, *ACS Nano*, 2016, **10**, 4695–4703.
12 W. Aftab, A. Mahmood, W. Guo, M. Yousaf, H. Tabassum, X. Huang, Z. Liang, A. Cao and R. Zou, *Energy Storage Mater*, 2019, **20**, 401–409.
13 H. Tabassum, X. Huang, R. Chen and R. Zou, *J. Materiomics*, 2015, **1**, 229–235.
14 L. Chen, R. Zou, W. Xia, Z. Liu, Y. Shang, J. Zhu, Y. Wang, J. Lin, D. Xia and A. Cao, *ACS Nano*, 2012, **6**, 10884–10892.
15 H. Zhang, Q. Sun, Y. Yuan, Z. Zhang and X. Cao, *Chem. Eng. J.*, 2018, **336**, 342–351.
16 W. Wu, X. Huang, K. Li, R. Yao, R. Chen and R. Zou, *Appl. Energy*, 2017, **190**, 474–480.
17 Y. Zhou, X. Wang, X. Liu, D. Sheng, F. Ji, L. Dong, S. Xu, H. Wu and Y. Yang, *Carbon*, 2019, **142**, 558–566.

18 R. Chen, R. Yao, W. Xia and R. Zou, *Appl. Energy*, 2015, **152**, 183–188.
19 M. M. Umair, Y. Zhang, K. Iqbal, S. Zhang and B. Tang, *Appl. Energy*, 2019, **235**, 846–873.
20 F. Xue, Y. Lu, X. Qi, J. Yang and Y. Wang, *Chem. Eng. J.*, 2019, **365**, 20–29.
21 X. Wei, F. Xue, X. Qi, J. Yang, Z. Zhou, Y. Yuan and Y. Wang, *Appl. Energy*, 2019, **236**, 70–80.
22 R. Cao, S. Chen, Y. Wang, N. Han, H. Liu and X. Zhang, *Carbon*, 2019, **149**, 263–272.
23 Z. Liu, R. Zou, Z. Lin, X. Gui, R. Chen, J. Lin, Y. Shang and A. Cao, *Nano Lett.*, 2013, **13**, 4028–4035.
24 G. Li, X. Zhang, J. Wang and J. Fang, *J. Mater. Chem. A*, 2016, **4**, 17042–17049.
25 M. Maleki, H. Karimian, M. Shokouhimehr, R. Ahmadi, A. Valanezhad and A. Beitollahi, *Chem. Eng. J.*, 2019, **362**, 469–481.
26 Y. Wu, C. Chen, Y. Jia, J. Wu, Y. Huang and L. Wang, *Appl. Energy*, 2018, **210**, 167–181.
27 W.-W. Li, W.-L. Cheng, B. Xie, N. Liu and L.-S. Zhang, *Energy Convers. Manage.*, 2017, **149**, 1–12.
28 W. Wu, W. Wu and S. Wang, *Appl. Energy*, 2019, **236**, 10–21.
29 J. Jing, H. Wu, Y. Shao, X. Qi, J. Yang and Y. Wang, *ACS Appl. Mater. Interfaces*, 2019, **11**, 19252–19259.
30 H. Wu, R. Chen, Y. Shao, X. Qi, J. Yang and Y. Wang, *ACS Sustainable Chem. Eng.*, 2019, **7**, 13532–13542.
31 Z. Zheng, X. Zhang, F. Pei, Y. Dai, X. Fang, T. Wang and N. Zheng, *J. Mater. Chem. A*, 2015, **3**, 19800–19806.
32 D. G. Atinafu, W. Dong, C. Wang and G. Wang, *J. Mater. Chem. A*, 2018, **6**, 8969–8977.
33 X. Huang, W. Xia and R. Zou, *J. Mater. Chem. A*, 2014, **2**, 19963–19968.
34 C. Yan, Z. Yu and B. Yang, *Fibers Polym.*, 2013, **14**, 1290–1294.
35 Y. Lu, X. Xiao, J. Fu, C. Huan, S. Qi, Y. Zhan, Y. Zhu and G. Xu, *Chem. Eng. J.*, 2019, **355**, 532–539.
36 Y. Lu, X. Xiao, J. Mo, C. Huan, S. Qi, Y. Zhan, Y. Zhu and G. Xu, *Colloids Surf., A*, 2018, **555**, 501–506.
37 S. Sirohi, D. Singh, R. Nain, D. Parida, A. K. Agrawal and M. Jassal, *RSC Adv.*, 2015, **5**, 34377–34382.
38 R. Perez-Masia, A. Lopez-Rubio, M. J. Fabra and J. M. Lagaron, *J. Appl. Polym. Sci.*, 2013, **130**, 3251–3262.
39 L. Zhao, J. Luo, Y. Li, H. Wang, G. Song and G. Tang, *J. Appl. Polym. Sci.*, 2017, **134**, 45538.
40 Y. Wan, P. Zhou, Y. Liu and H. Chen, *RSC Adv.*, 2016, **6**, 21204–21209.
41 Y. Lu, X. Xiao, Y. Zhan, C. Huan, S. Qi, H. Cheng and G. Xu, *ACS Appl. Mater. Interfaces*, 2018, **10**, 12759–12767.
42 X. Guo, C. Liu, N. Li, S. Zhang and Z. Wang, *Ind. Eng. Chem. Res.*, 2018, **57**, 15697–15702.

